

Adaptation of an Electrochemistry-based Li-Ion Battery Model to Account for Deterioration Observed Under Randomized Use

Brian Bole¹, Chetan S. Kulkarni¹, Matthew Daigle²

¹ SGT, Inc., NASA Ames Research Center, Moffett Field, CA 94035

brian.bole@nasa.gov, chetan.kulkarni@nasa.gov

² NASA Ames Research Center, Moffett Field, CA 94035

matthew.j.daigle@nasa.gov

ABSTRACT

Tracking the variation in battery dynamics as a function of health is presently attracting attention in academia and industry due to the increased usage of expensive batteries in dynamic systems such as aircraft and electric cars. The online adaptation of battery models to account for age-dependent changes in dynamics is necessary to maintain accurate estimates of the remaining system operations that can be supported under battery power. A novel method for the adaptation of parameters in an electrochemical model of a lithium-ion battery is presented here. An unscented Kalman filtering algorithm is shown to enable the production of internal battery state estimates and age-dependent electrochemical model parameter estimates using only battery current and voltage data collected over randomized discharge profiles. The use of only data collected over randomized discharge profiles distinguishes this work from other works that make use of reference discharge cycles to judge battery health. The experimental results presented here compare online model estimates produced by the proposed algorithm to offline model estimates obtained by periodically taking batteries offline to run reference discharge cycles.

1. INTRODUCTION

Continued improvements in battery cost, efficiency, and power density have resulted in their increasing use in critical applications such as aircraft and electric cars. In such applications, it is necessary to maintain an accurate model of battery capabilities over many years of use. With an accurate model, precise predictions of end-of-discharge predictions can be made along with predictions of the remaining system operational time that can be supported under battery power (Daigle & Kulkarni, 2013; Saha, Goebel, Poll, &

Christophersen, 2009). However, batteries age with increased use, and in order to continue to make accurate predictions, approaches to track of age-dependent changes in battery dynamics are necessary (Saha et al., 2009). While some research has been performed to understand the dynamics of battery aging (Ning & Popov, 2004; Ning, White, & Popov, 2006), relatively little work has been performed to develop approaches for tracking battery age online (Saha & Goebel, 2009).

Modeling methodologies used to represent battery dynamics are generally classified as follows: (i) empirical models; (ii) electrochemical engineering models; (iii) multi-physics models; and (iv) molecular/atomist models (Ramadesigan et al., 2012). Empirical models are based on fitting certain functions to past experimental data, without making use of any physicochemical principles. Electrochemical, multi-physics, and atomist models incorporate progressively more fine-grained representations of battery physics. Because more fine-grained models generally increase the model development cost and the cost of computation, it is desired to select a model granularity appropriate to an application's accuracy requirements and available resources (Daigle et al., 2011). In this paper, we use an electrochemistry-based lithium ion (Li-ion) battery model developed in (Daigle & Kulkarni, 2013). The electrochemical modeling used is at level of abstraction high enough that the model is still efficient while improving upon the fidelity of previous approaches (Saha & Goebel, 2009; Daigle et al., 2012; Oliva et al., 2013), which used empirical and equivalent circuit battery models.

The use of unscented Kalman filtering (UKF) (Julier & Uhlmann, 2004) to make online corrections to battery state estimates based on online battery voltage measurements has been described in several recent publications (Daigle & Kulkarni, 2014; Bole et al., 2013; Oliva et al., 2013). The addition of a filtering routine for closed-loop state estimation mitigates the accumulation of model error over time as is seen in open-loop state estimation methods such as the commonly

Brian Bole et al. This is an open-access article distributed under the terms of the Creative Commons Attribution 3.0 United States License, which permits unrestricted use, distribution, and reproduction in any medium, provided the original author and source are credited.

used method of coulomb counting (Dai et al., 2006). This paper demonstrates the use of UKF not only to estimate the states in an electrochemistry model that vary over a charge-discharge cycle, but also to adapt certain parameters in the model that are known to change as a function of battery age.

While some research has been performed to understand the dynamics of battery aging (Ning & Popov, 2004; Ning et al., 2006), relatively little work has been performed to develop approaches for tracking battery age online (Saha & Goebel, 2009). Generally, a progressive reduction in charge storage capacity and an increase in internal resistance are both known to occur as the battery ages. These changes are typically estimated by comparing the voltage dynamics of healthy and aged batteries over a reference current profile (Broussely et al., 2005). Estimating the state of age-dependent battery parameters from the current-voltage dynamics of batteries in operation is a more challenging proposition than estimating parameters using reference cycles, because individual runs are less able to be directly compared. This paper introduces experimental results for an algorithm that uses only randomized discharging data to track battery states and estimate model parameters. The experimental results presented here compare online model estimates produced by the proposed algorithm to offline model estimates obtained by periodically taking batteries offline to run reference discharge cycles.

This paper is organized as follows. The electrochemistry-based lithium ion battery model is summarized in Section 2. Battery deterioration modes are discussed in Section 3. Sample results from a set of experiments that age batteries using randomized discharge profiles are introduced in Section 4. A UKF algorithm for online state estimation and age-dependent parameter identification over randomized battery usage periods is described in Section 5. Results generated by applying the UKF algorithm to randomized discharging data sets are summarized in Section 6. Finally, concluding remarks are given in Section 7.

2. BATTERY CHARGE AND DISCHARGE MODELING

A battery converts chemical energy into electrical energy, and often consists of many cells. A cell consists of a positive electrode and a negative electrode with electrolyte in which the ions can migrate. For Li-ion, a common chemistry is a positive electrode consisting of lithium cobalt oxide (Li_xCoO_2) and negative electrode of lithiated carbon (Li_xC). These active materials are bonded to metal-foil current collectors at both ends of the cell and electrically isolated by a micro-porous polymer separator film that is permeable to Li ions. The electrolyte enables lithium ions (Li^+) to diffuse between the positive and negative electrodes. The lithium ions insert or deinsert from the active material depending upon the electrode and whether the active process is charging or discharging, respectively.

This section introduces a battery model derived from a simplified set of electrochemical equations governing charge flow and voltage drops at the cathode, anode, and separator layers of a Li-ion battery. This model is described in detail in (Daigle & Kulkarni, 2013) and summarized here.

The voltage terms of the battery are expressed as functions of the amount of charge in the electrodes (the states of the model). Each electrode, positive (subscript p) and negative (subscript n), is split into two volumes, a surface layer (subscript s) and a bulk layer (subscript b). The differential equations for the battery describe how charge moves through these volumes. The charge (q) variables are described using

$$\dot{q}_{s,p} = i_{app} + \dot{q}_{bs,p} \quad (1)$$

$$\dot{q}_{b,p} = -\dot{q}_{bs,p} + i_{app} - i_{app} \quad (2)$$

$$\dot{q}_{b,n} = -\dot{q}_{bs,n} + i_{app} - i_{app} \quad (3)$$

$$\dot{q}_{s,n} = -i_{app} + \dot{q}_{bs,n}, \quad (4)$$

where i_{app} is the applied electric current. The term $\dot{q}_{bs,i}$ describes diffusion from the bulk to surface layer for electrode i , where $i = n$ or $i = p$.

$$\dot{q}_{bs,i} = \frac{1}{D}(c_{b,i} - c_{s,i}), \quad (5)$$

where D is the diffusion constant. The c terms are lithium ion concentrations:

$$c_{b,i} = \frac{q_{b,i}}{v_{b,i}} \quad (6)$$

$$c_{s,i} = \frac{q_{s,i}}{v_{s,i}}, \quad (7)$$

Here, $c_{v,i}$ is the concentration of charge in electrode i , and $v_{v,i}$ is the total volume of charge storage capability. We define $v_i = v_{b,i} + v_{s,i}$. Note now that the following relations hold:

$$q_p = q_{s,p} + q_{b,p} \quad (8)$$

$$q_n = q_{s,n} + q_{b,n} \quad (9)$$

$$q^{\max} = q_{s,p} + q_{b,p} + q_{s,n} + q_{b,n}. \quad (10)$$

We can also express mole fractions (x) based on the q variables:

$$x_i = \frac{q_i}{q^{\max}}, \quad (11)$$

$$x_{s,i} = \frac{q_{s,i}}{q_{s,i}^{\max}}, \quad (12)$$

$$x_{b,i} = \frac{q_{b,i}}{q_{b,i}^{\max}}, \quad (13)$$

where $q^{\max} = q_p + q_n$ refers to the total amount of available Li-ions. It follows that $x_p + x_n = 1$. For Li-ion batteries, when fully charged, $x_p = 0.4$ and $x_n = 0.6$. When fully discharged, $x_p = 1$ and $x_n = 0$ (Karthikeyan, Sikha, & White, 2008).

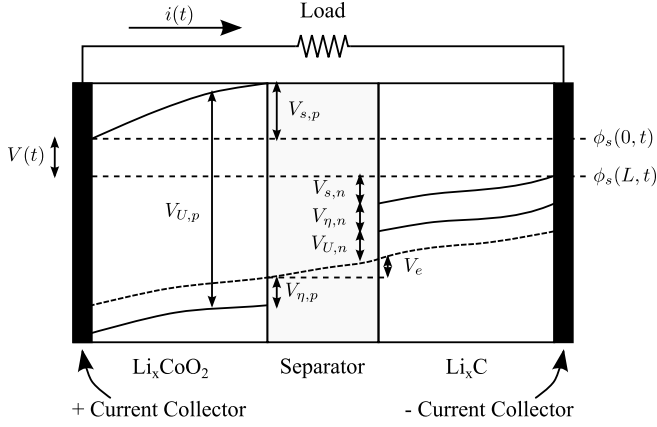


Figure 1. Battery voltages.

The different potentials are summarized in Fig. 1 (originally presented in (Daigle & Kulkarni, 2013) and adapted from (Rahn & Wang, 2013)). The overall battery voltage $V(t)$ is the difference between the potential at the positive current collector, $\phi_s(0, t)$, and the negative current collector, $\phi_s(L, t)$, minus resistance losses at the current collectors (not shown in the diagram). At the positive current collector is the equilibrium potential $V_{U,p}$. This voltage is then reduced by $V_{s,p}$, due to the solid-phase ohmic resistance, and $V_{\eta,p}$, the surface overpotential. The electrolyte ohmic resistance then causes another drop V_e . At the negative electrode, there is a drop $V_{\eta,n}$ due to the surface overpotential, and a drop $V_{s,n}$ due to the solid-phase resistance. The voltage drops again due to the equilibrium potential at the negative current collector $V_{U,n}$. These voltages are described by the following set of equations:

$$V_{U,i} = U_0 + \frac{RT}{nF} \ln \left(\frac{1 - x_{s,i}}{x_{s,i}} \right) + V_{\text{INT},i}, \quad (14)$$

$$V_{\text{INT},i} = \frac{1}{nF} \left(\sum_{k=0}^{N_i} A_{i,k} \left((2x_i - 1)^{k+1} - \frac{2x_i k (1 - x_i)}{(2x_i - 1)^{1-k}} \right) \right), \quad (15)$$

$$V_o = i_{\text{app}} R_o, \quad (16)$$

$$V_{\eta,i} = \frac{RT}{F\alpha} \operatorname{arcsinh} \left(\frac{J_i}{2J_{i0}} \right), \quad (17)$$

$$J_i = \frac{i}{S_i}, \quad (18)$$

$$J_{i0} = k_i (1 - x_{s,i})^\alpha (x_{s,i})^{1-\alpha}, \quad (19)$$

$$V = V_{U,p} - V_{U,n} - V'_o - V'_{\eta,p} - V'_{\eta,n}, \quad (20)$$

$$\dot{V}'_o = (V_o - V'_o) / \tau_o \quad (21)$$

$$\dot{V}'_{\eta,p} = (V_{\eta,p} - V'_{\eta,p}) / \tau_{\eta,p} \quad (22)$$

$$\dot{V}'_{\eta,n} = (V_{\eta,n} - V'_{\eta,n}) / \tau_{\eta,n}. \quad (23)$$

Here, U_0 is a reference potential, R is the universal gas constant, T is the electrode temperature (in K), n is the number

of electrons transferred in the reaction ($n = 1$ for Li-ion), F is Faraday's constant, J_i is the current density, and J_{i0} is the exchange current density, k_i is a lumped parameter of several constants including a rate coefficient, electrolyte concentration, and maximum ion concentration. $V_{\text{INT},i}$ is the activity correction term (0 in the ideal condition). We use the Redlich-Kister expansion with $N_p = 12$ and $N_n = 0$ (see (Daigle & Kulkarni, 2013)). The τ parameters are empirical time constants (used since the voltages do not change instantaneously).

This model contains as states $q_{s,p}$, $q_{b,p}$, $q_{b,n}$, $q_{s,n}$, V'_o , $V'_{\eta,p}$, and $V'_{\eta,n}$. The single model output is V . Parameter values for a typical Li-ion cell are given in (Daigle & Kulkarni, 2013).

The state of charge (SOC) of a battery is defined to be 1 when the battery is fully charged and 0 when the battery is fully discharged by convention. In this model, it is analogous to the mole fraction x_n , but scaled from 0 to 1. We distinguish here between nominal SOC and *apparent* SOC (Daigle & Kulkarni, 2013). Nominal SOC is computed based on the combination of the bulk and surface layer control volumes in the negative electrode, whereas apparent SOC is computed based only on the surface layer. When a battery reaches the voltage cutoff, apparent SOC is 0, and nominal SOC is greater than 0 (how much greater depends on the difference between the diffusion rate and the current drawn). Once the concentration gradient settles out, the surface layer will be partially replenished and apparent SOC will rise while nominal SOC remains the same. Nominal (SOC_n) and apparent (SOC_a) SOC are defined using

$$\text{SOC}_n = \frac{q_n}{0.6q^{\max}} \quad (24)$$

$$\text{SOC}_a = \frac{q_{s,n}}{0.6q^{\max_{s,n}}}, \quad (25)$$

where $q^{\max_{s,n}} = q^{\max} \frac{v_{s,n}}{v_n} \cdot 1$.

3. BATTERY DETERIORATION MODELING

The rate of deterioration of a battery depends on the chemistry, charge-discharge cycling, temperature, and storage conditions, among other factors. Some relevant physical aging mechanisms observed in batteries are:

1. Solid-electrolyte interface (SEI) layer growth: The negative electrode degrades with the growth of the SEI layer leading to an increase in the impedance. The layers are formed during cycling and storage at high temperatures and entrains the lithium.
2. Lithium corrosion: Lithium in the active carbon material of the negative electrode corrodes over time leading to

¹Note that SOC of 1 corresponds to the point where $q_n = 0.6q^{\max_{s,n}}$, since the mole fraction at the positive electrode cannot go below 0.4, as described earlier.

degradation. This causes a decrease in the capacity due to irreversible loss of mobile lithium ions.

3. Lithium plating: At low temperatures, high charge rates and low cell voltages form a plating layer on the negative electrode that leads to irreversible loss of lithium.
4. Contact loss: The SEI layer disconnects from the negative electrode, which leads to contact loss and an increase in impedance.
5. Diffusion Stress: Changes in diffusion properties may lead to changes in the charge and discharge times, apparent capacity and impedance.

The various battery aging modes manifest in two major changes to battery electrochemical dynamics. The first is a loss of capacity due to parasitic and side reactions that result in a loss of active (mobile) Li ions. The second is an increase in internal resistance due to SEI layer growth and other factors. Other, less significant, changes to battery electrochemical dynamics are not considered here because the added computational costs are considered to outweigh the benefit to model accuracy. (Ning et al., 2006) looked into loss of active lithium and increase in resistance under constant loading conditions. In this work we look at degradation observed under random loading conditions.

In the battery model, the total available charge in the battery is represented through q^{\max} . Therefore, the loss of active material can be represented in the model through a change in q^{\max} (Daigle & Kulkarni, 2013). The R_o parameter captures a constant ohmic drop that does not vary as a function of battery charge.

Figure 2 shows plots of model fitting with a new and aged battery after adding adjustments to the q^{\max} and R_o terms. The figures clearly show the need to tune these parameters to capture the modified electrochemical dynamics of a degraded battery. However, it should also be noted that the fit shown in Figure 2(d) could be improved to a lesser extent by adapting additional terms. The authors suggest that readers interested in adapting additional terms in the electrochemical model start by considering the diffusion rate between the bulk layer and surface layer (D in Eq. (5)). See (Park, Zhang, Chung, Less, & Sastry, 2010) for a discussion of age-related changes to the diffusion rate.

4. A BATTERY AGING EXPERIMENT

This section introduces a battery aging experiment. Battery aging is performed here by repeatedly charging battery cells to approximately 100% SOC (≈ 4.2 V) and then discharging them to 3.2 V using a randomized sequence of current loads ranging from 0.5A to 4A. The sequence is randomized in order to better represent practical battery usage. After every fifty randomized discharging cycles, an offline characteriza-

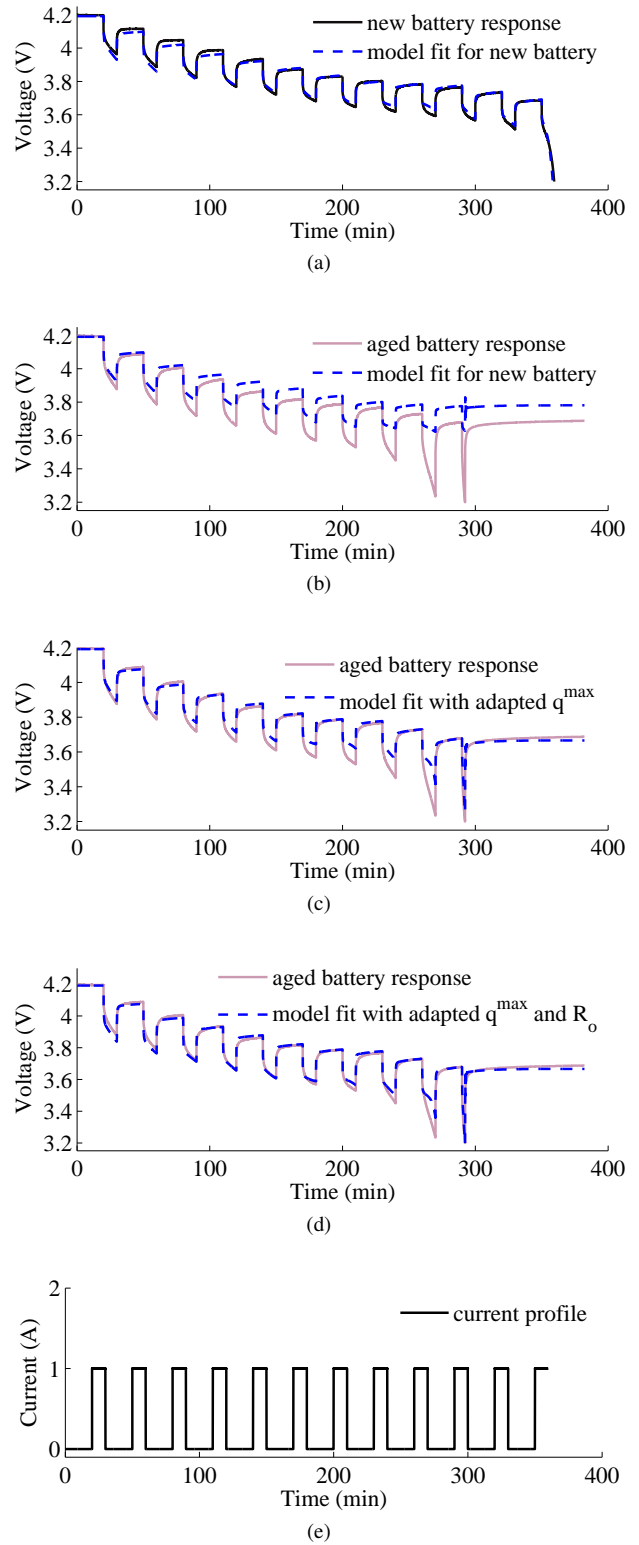


Figure 2. Sample model fitting results for a new battery (a), and an aged battery (b)-(d). The loading profiles used are shown in (e).

Battery Cycling Procedure:*top:**pulsed load characterization:*

fully charge to 4.2V

while voltage > 3.2V

rest for 20 min

load at 1A for 10 min

end while $j = 0$ *random walk aging:***while** $j < 50$

fully charge to 4.2V

while voltage > 3.2V $I = \text{rand}[0.5, 1, 1.5, 2, 2.5, 3, 3.5, 4]$ load at I for 5 min**end while** $j = j + 1$ **end while****goto:** *top*

Figure 3. Procedure used for battery aging and periodic characterization

tion of the q^{max} and R_o model parameters is performed using the pulsed load cycle described in the previous section.

The battery cycling procedure that is used to age individual battery cells and periodically recharacterize health dynamics is outlined in Fig. 3. Fig. 4 shows battery current and voltage for pulsed load characterization cycles taken periodically over about 6 months of continuous battery cycling. Later pulsed load cycles are plotted with lighter line shading.

Age-dependent changes in battery dynamics are denoted with arrows in the figure. The battery voltage is seen to reach the 3.2V cutoff earlier as the battery ages. Aged batteries are also seen to settle to a higher resting voltage after the pulsed profile completes. Both phenomenon can be explained by a decreasing trend in battery capacity and an increasing trend in internal resistance.

Battery capacity loss will result in a decrease in available Li-ions, and therefore a faster discharge time for a given output current, which causes a lowering of surface and bulk battery potentials, see Eqs. (11)-(23). An increase in internal resistance will cause a proportional decrease in battery voltage, see Eq. (16). An increased voltage drop due to an increase in battery internal resistance will also cause the battery voltage to reach the voltage cut-off threshold at a higher SOC, resulting in the higher resting battery voltage measurements seen in Fig. 4.

Fig. 5 shows estimates of q^{max} and R_o obtained by performing an offline least squares fit of the actual and modeled bat-

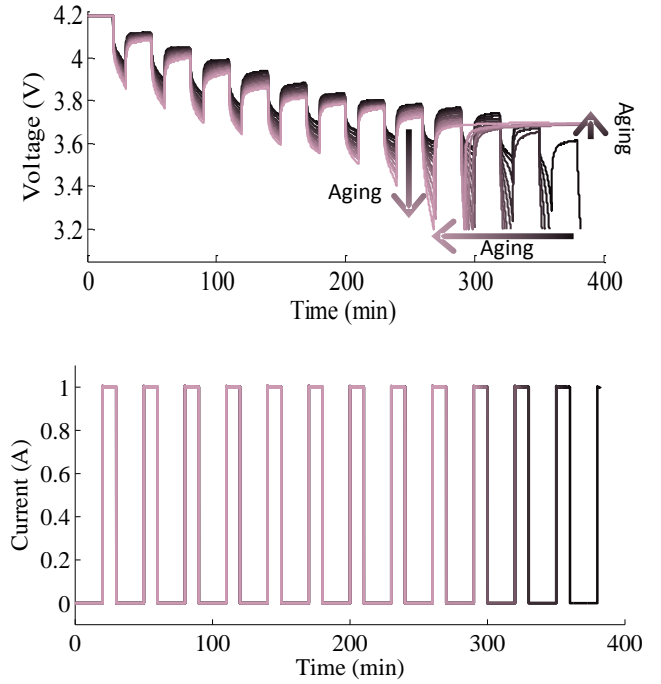


Figure 4. Pulsed voltage profiles recorded periodically over 3 months of continuous battery use.

Table 1. Statistics of linear regression fit for q^{max} and R_o

	m_0	m_1	σ^2	R^2
q^{max}	-8.11×10^{-4}	2.15	9.33×10^5	0.96
R_o	1.25×10^{-4}	1.05×10^{-1}	1.4×10^{-3}	0.94

ttery voltage over periodic pulsed load characterization cycles. The fitted parameter values are plotted against the integral of battery discharge current, in order to observe the relationship between battery usage and parameter change.

A first-order regression model is considered here as a rough approximation of parameter dependence on use. Table 1 shows the slope (denoted m_0), y-intercept (denoted m_1), variance (denoted σ^2), and coefficient of determination (denoted R^2), for the fitted q^{max} and R_o parameters. The coefficient of determination is a normalized measure $\in [0, 1]$ that indicates how well the regression fits the data. A coefficient of determination greater than 0.9 indicates a fairly good model fit. The R^2 values for q^{max} and R_o linear regressions are both seen to exceed this benchmark.

A discussion of battery deterioration modeling and end of useful life prediction using such a model is beyond the scope of this paper. The reader is also cautioned that the battery deterioration observed here is expected to be strongly dependent on the design of experiments.

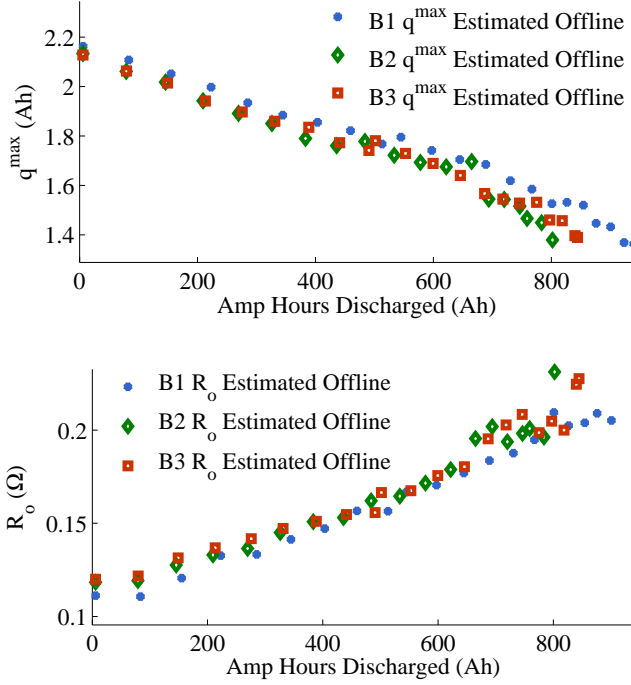


Figure 5. Parameter fitting results for q^{max} and R_o captured periodically over three months of continuous use.

5. ONLINE STATE ESTIMATION AND PARAMETER IDENTIFICATION

An unscented Kalman filter (UKF) (Julier & Uhlmann, 1997, 2004) is introduced here to make corrective updates to the internal state estimates in the battery model in addition to the age-dependent q^{max} and R_o parameters. Among nonlinear filters, the UKF generally has better accuracy than the extended Kalman filter, and avoids the high computational cost of particle filters (Arulampalam, Maskell, Gordon, & Clapp, 2002). We summarize the filter basics here; more details may be found in (Julier & Uhlmann, 1997, 2004).

The UKF assumes the general nonlinear form of the state and output equations, but is restricted to additive Gaussian noise. First, n_s sigma points $\hat{\mathbf{x}}_{k-1|k-1}^i$ are derived from the current mean $\hat{\mathbf{x}}_{k-1|k-1}$ and covariance estimates $\mathbf{P}_{k-1|k-1}$. The prediction step is:

$$\hat{\mathbf{x}}_{k|k-1}^i = \mathbf{f}(\hat{\mathbf{x}}_{k-1|k-1}^i, \mathbf{u}_{k-1}), i = 1, \dots, n_s \quad (26)$$

$$\hat{\mathbf{y}}_{k|k-1}^i = \mathbf{h}(\hat{\mathbf{x}}_{k|k-1}^i), i = 1, \dots, n_s \quad (27)$$

$$\hat{\mathbf{x}}_{k|k-1} = \sum_{i=1}^{n_s} w^i \hat{\mathbf{x}}_{k|k-1}^i \quad (28)$$

$$\hat{\mathbf{y}}_{k|k-1} = \sum_{i=1}^{n_s} w^i \hat{\mathbf{y}}_{k|k-1}^i \quad (29)$$

$$\mathbf{P}_{k|k-1} = \mathbf{Q} +$$

$$\sum_{i=1}^{n_s} w^i (\mathbf{x}_{k|k-1}^i - \hat{\mathbf{x}}_{k|k-1})(\mathbf{x}_{k|k-1}^i - \hat{\mathbf{x}}_{k|k-1})^T, \quad (30)$$

where \mathbf{Q} is the process noise covariance matrix.

The update step is:

$$\mathbf{P}_{yy} = \mathbf{R} + \sum_{i=1}^{n_s} w^i (\mathbf{y}_{k|k-1}^i - \hat{\mathbf{y}}_{k|k-1})(\mathbf{y}_{k|k-1}^i - \hat{\mathbf{y}}_{k|k-1})^T \quad (31)$$

$$\mathbf{P}_{xy} = \sum_{i=1}^{n_s} w^i (\mathbf{x}_{k|k-1}^i - \hat{\mathbf{x}}_{k|k-1})(\mathbf{y}_{k|k-1}^i - \hat{\mathbf{y}}_{k|k-1})^T \quad (32)$$

$$\mathbf{K}_k = \mathbf{P}_{xy} \mathbf{P}_{yy}^{-1} \quad (33)$$

$$\hat{\mathbf{x}}_{k|k} = \hat{\mathbf{x}}_{k|k-1} + \mathbf{K}_k (\mathbf{y}_k - \hat{\mathbf{y}}_{k|k-1}) \quad (34)$$

$$\mathbf{P}_{k|k} = \mathbf{P}_{k|k-1} - \mathbf{K}_k \mathbf{P}_{yy} \mathbf{K}_k^T, \quad (35)$$

where \mathbf{R} is the sensor noise covariance matrix.

The use of the UKF for closed-loop state updates of the 7 states in the battery model described in Section 2, was presented in (Daigle & Kulkarni, 2013). The UKF algorithm presented in (Daigle & Kulkarni, 2013) was updated for use here by considering the R_o parameter in Eq. 16 as an additional state to be updated online by the UKF.

An additional outer-loop process is then used to infer q^{max} values that correspond to a given window of SOC_n estimates under known battery loading conditions. We elected to use an outer-loop estimation process for q^{max} , rather than including it in the UKF because it is straightforward to infer q^{max} from SOC_n estimates. This is seen by first rewriting the SOC_n definition, given in Eq. (24), in terms of a UKF-based estimate of q_n .

$$\widehat{SOC}_n(t) = \frac{\hat{q}_n(t)}{0.6q^{max}}, \quad (36)$$

where $\hat{q}_n(t)$ represents an estimate of q_n at time t , and $\widehat{SOC}_n(t)$ represents a subsequently derived estimate of SOC_n . The difference in \widehat{SOC}_n estimates of over a given time window is then expressed as:

$$\widehat{SOC}_n \Big|_{t_0}^t = \frac{\hat{q}_n|_{t_0}^t}{0.6q^{max}}. \quad (37)$$

Next, consider that the true value of $q_n|_{t_0}^t$ is equal to the amount of charge flow into or out of the battery over the given time window.

$$q_n|_{t_0}^t = \int_{t_0}^t i_{app}, \quad (38)$$

where i_{app} represents the net current into or out of the battery.

A substitution of Eq. (38) into Eq. (37) yields an inferred estimate of q^{max} .

$$\hat{q}^{max}(t) = \frac{q_n|_{t_0}^t}{0.6 \widehat{SOC}_n|_{t_0}^t}, \quad (39)$$

where $\hat{q}^{max}(t)$ represents an estimate of the q^{max} model parameter at time t .

6. RESULTS

Fig. 6(a) shows an example of the online adaptation of battery state estimates and model parameters in order to match the measured voltage response of an aged battery over a randomized discharge cycle. The predicted voltage response for a new battery, and the voltage estimation output of a UKF-based observer initialized with the parameters of a new battery are also plotted in Fig. 6(a). Online UKF estimates of the q^{max} and R_o parameters are shown in Figs. 6(b) and (c). The randomized loading profile used in this example is shown in Fig. 6(d).

The battery voltage output estimates from the UKF are seen to converge to match the measured voltage estimates over the 40 minute randomized discharging cycle. The variation seen in the q^{max} and R_o estimates from 0 to 40 minutes is due primarily to the large initial disparity between the parameters fitted for a new battery model and the model parameters needed to explain the dynamics of an aged battery. Typically, the model parameters estimated by the UKF over a previous discharge cycle would be used to initialize the battery model for the following discharge cycle. This would lead to a much smaller error in the initial parameter estimates and less parameter variation would result.

Fig. 7 shows online q^{max} and R_o estimates produced by the UKF observer over successive randomized discharge cycles. The offline estimates of q^{max} and R_o that were originally shown in Fig. 5 are also plotted in Fig. 7 for comparison. The online q^{max} estimates are seen in Fig. 7 to track the offline q^{max} estimates very closely. This indicates not only that the UKF is able to track battery capacity over randomized discharging cycles, but also that the online battery SOC estimates that are used to calculate capacity (see Eqs. (36)-(39)) are also tracking the true battery SOC over randomized usage.

Online R_o estimates are seen in Fig. 7 to be noticeably lower and more non-linear than the offline R_o estimates. Despite this discrepancy, online R_o estimates display some similarities to the offline estimates. Both sets of R_o estimates tend to be monotonically increasing with battery age, and both show a slightly lower resistance estimate for battery B1 than for B2 and B3. The bias observed between offline and online estimates can be attributed primarily to a difficulty in setting up the process noise covariance matrix, \mathbf{Q} , in the UKF to filter

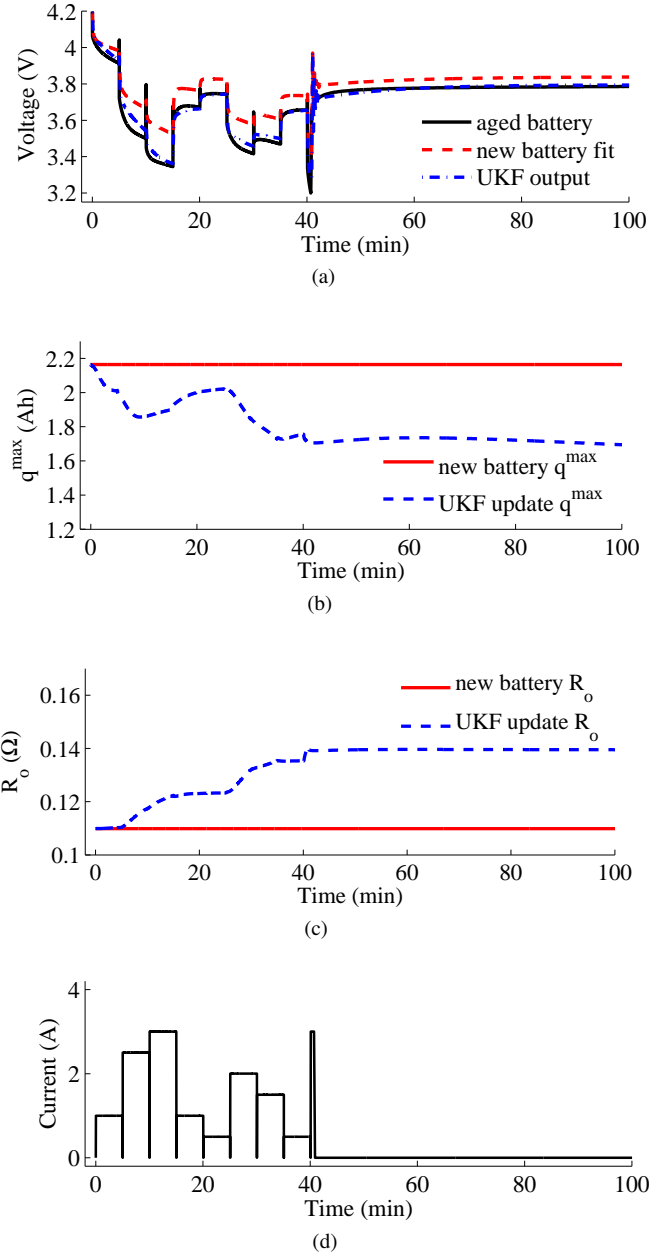


Figure 6. The measured voltage response of an aged battery over a randomized discharge cycle, the predicted voltage response for a new battery, and the voltage estimation output of a UKF-based observer are shown in (a). Online estimates of the q^{max} and R_o parameters are shown in (b) and (c). The loading profile used is shown in (d).

out the effects of the R_o term from those of the other parameters in state vector. It is certain that a refinement of \mathbf{Q} could improve the tracking performances observed for the q^{max} and R_o parameters. However, the non-optimized tracking performance shown here is sufficient to demonstrate the feasibility of the proposed approach for model adaptation over variable battery usage.

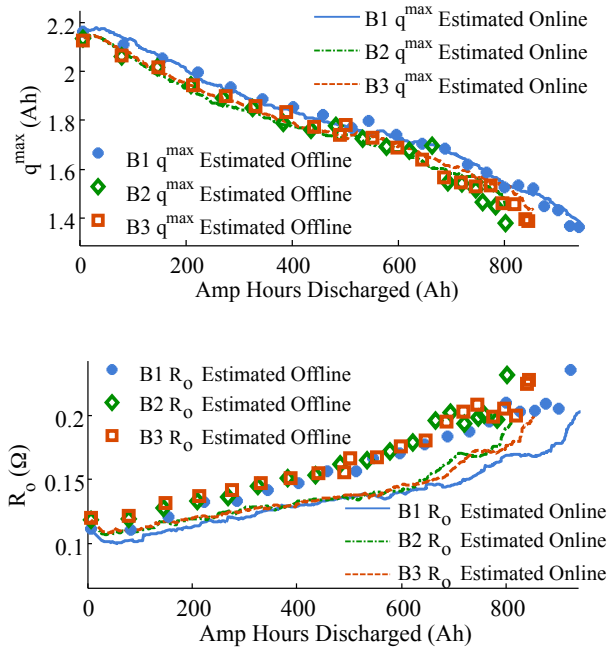


Figure 7. Online and offline estimates of q^{\max} and R_o model parameters.

7. CONCLUSIONS

An approach for the online tracking of age-dependent changes in battery dynamics was presented. An electrochemistry-based Li-ion battery model was shown to relate known age-dependent electrochemical phenomena to changes in battery input-output dynamics observed over randomized battery usage. A battery aging experiment was introduced, and an unscented Kalman filtering algorithm was shown to track age-dependent changes in battery model parameters over successive randomized battery discharging profiles.

In future work the battery state of health tracking approach presented here may be extended to the online prediction of remaining useful life. This would require additional modeling of the underlying physics of battery degradation as a function of usage. Linear regression models for battery capacity and internal resistance change as a function of energy discharged are analyzed here as a starting point for this future work.

ACKNOWLEDGMENT

The project support by NASA's AvSafe/SSAT and OCT/ACLO are respectfully acknowledged.

REFERENCES

Arulampalam, M. S., Maskell, S., Gordon, N., & Clapp, T. (2002). A tutorial on particle filters for on-

- line nonlinear/non-Gaussian Bayesian tracking. *IEEE Transactions on Signal Processing*, 50(2), 174–188.
- Bole, B., Teubert, C., Chi, Q. C., Edward, H., Vazquez, S., Goebel, K., & Vachtsevanos, G. (2013). SIL/HIL replication of electric aircraft powertrain dynamics and inner-loop control for V&V of system health management routines. In *Annual conference of the prognostics and health management society*.
- Broussely, M., Biensan, P., Bonhomme, F., Blanchard, P., Herreyre, S., Nechev, K., & Staniewicz, R. (2005). Main aging mechanisms in li ion batteries. *Journal of Power Sources*, 146(1-2), 90-96.
- Dai, H., Wei, X., & Sun, Z. (2006). Online soc estimation of high-power Lithium-Ion batteries used on HEVs. In *IEEE international conference on vehicular electronics and safety*.
- Daigle, M., & Kulkarni, C. (2013, October). Electrochemistry-based battery modeling for prognostics. In *Annual conference of the prognostics and health management society 2013* (p. 249-261).
- Daigle, M., & Kulkarni, C. (2014). A battery health monitoring framework for planetary rovers. In *Proceedings of the IEEE aerospace conference*.
- Daigle, M., Roychoudhury, I., Narasimhan, S., Saha, S., Saha, B., & Goebel, K. (2011, September). Investigating the effect of damage progression model choice on prognostics performance. In *Proceedings of the annual conference of the prognostics and health management society 2011* (p. 323-333).
- Daigle, M., Saxena, A., & Goebel, K. (2012, September). An efficient deterministic approach to model-based prediction uncertainty estimation. In *Annual conference of the prognostics and health management society* (p. 326-335).
- Julier, S. J., & Uhlmann, J. K. (1997). A new extension of the Kalman filter to nonlinear systems. In *Proceedings of the 11th international symposium on aerospace/defense sensing, simulation and controls* (pp. 182–193).
- Julier, S. J., & Uhlmann, J. K. (2004, Mar). Unscented filtering and nonlinear estimation. *Proceedings of the IEEE*, 92(3), 401–422.
- Karthikeyan, D. K., Sikha, G., & White, R. E. (2008). Thermodynamic model development for lithium intercalation electrodes. *Journal of Power Sources*, 185(2), 1398–1407.
- Ning, G., & Popov, B. N. (2004). Cycle life modeling of lithium-ion batteries. *Journal of The Electrochemical Society*, 151(10), A1584–A1591.
- Ning, G., White, R. E., & Popov, B. N. (2006). A generalized cycle life model of rechargeable li-ion batteries. *Electrochimica Acta*, 51(10), 2012–2022.
- Oliva, J., Weihrauch, C., & Bertram, T. (2013, October). A model-based approach for predicting the remaining

driving range in electric vehicles. In *Annual conference of the prognostics and health management society 2013* (p. 438-448).

- Park, M., Zhang, X., Chung, M., Less, G. B., & Sastry, A. M. (2010). A review of conduction phenomena in li-ion batteries. *Journal of Power Sources*, 195(24), 7904–7929.
- Rahn, C. D., & Wang, C.-Y. (2013). *Battery systems engineering*. Wiley.
- Ramadesigan, V., Northrop, P. W., De, S., Santhanagopalan, S., Braatz, R. D., & Subramanian, V. (2012). Modeling and simulation of lithium-ion batteries from a systems engineering perspective. *Journal of The Electrochemical Society*, 159(3), R31–R45.
- Saha, B., & Goebel, K. (2009, September). Modeling Li-ion battery capacity depletion in a particle filtering framework. In *Proceedings of the annual conference of the prognostics and health management society 2009*.
- Saha, B., Goebel, K., Poll, S., & Christophersen, J. (2009, February). Prognostics methods for battery health monitoring using a Bayesian framework. *IEEE Transactions on Instrumentation and Measurement*, 58(2), 291–296.

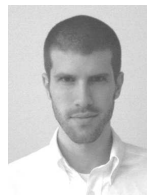
BIOGRAPHIES



Brian M. Bole graduated from the FSU-FAMU School of Engineering with a B.S. in Electrical and Computer Engineering and a B.S. in Applied Math. Brian received M.S. and Ph.D. degrees in Electrical Engineering from the Georgia Institute of Technology. His research interests include: analysis of stochastic processes, risk analysis, and optimization of stochastic systems. Brian is currently investigating the use of risk management and stochastic optimization techniques for prognostics and prognostics-informed decision making in robotic and aviation applications. From 2011 to 2013 he performed joint research with the Prognostic Center of Excellence at NASA Ames under the NASA graduate student research fellowship. He is currently working as a research engineer for Stinger Ghaffarian Technologies and is conducting joint research with the intelligent systems division at NASA Ames.



Chetan S. Kulkarni received the B.E. (Bachelor of Engineering) degree in Electronics and Electrical Engineering from University of Pune, India in 2002 and the M.S. and Ph.D. degrees in Electrical Engineering from Vanderbilt University, Nashville, TN, in 2009 and 2013, respectively. He was a Senior Project Engineer with Honeywell Automation India Limited (HAIL) from 2003 till April 2006. From May 2006 to August 2007 he was a Research Fellow at the Indian Institute of Technology (IIT) Bombay with the Department of Electrical Engineering. From Aug 2007 to Dec 2012, he was a Graduate Research Assistant with the Institute for Software Integrated Systems and Department of Electrical Engineering and Computer Science, Vanderbilt University, Nashville, TN. Since Jan 2013 he has been a Staff Researcher with SGT Inc. at the Prognostics Center of Excellence, NASA Ames Research Center. His current research interests include physics-based modeling, model-based diagnosis and prognosis. Dr. Kulkarni is a member of the Prognostics and Health Management (PHM) Society, AIAA and the IEEE.



Matthew Daigle received the B.S. degree in Computer Science and Computer and Systems Engineering from Rensselaer Polytechnic Institute, Troy, NY, in 2004, and the M.S. and Ph.D. degrees in Computer Science from Vanderbilt University, Nashville, TN, in 2006 and 2008, respectively. From September 2004 to May 2008, he was a Graduate Research Assistant with the Institute for Software Integrated Systems and Department of Electrical Engineering and Computer Science, Vanderbilt University, Nashville, TN. From June 2008 to December 2011, he was an Associate Scientist with the University of California, Santa Cruz, at NASA Ames Research Center. Since January 2012, he has been with NASA Ames Research Center as a Research Computer Scientist. His current research interests include physics-based modeling, model-based diagnosis and prognosis, simulation, and hybrid systems.